A PRIMITIVE-VARIABLE NODAL METHOD FOR THE TIME-DEPENDENT NAVIER-STOKES EQUATIONS

E. P. E. Michael and J. Dorning
University of Virginia
Charlottesville, VA 22903-2442
eem7g@virginia.edu, dorning@virginia.edu

Keywords: Numerical methods, nodal methods, computational fluid dynamics, Navier-Stokes equations.

ABSTRACT

A new primitive-variable nodal integral method for the time-dependent, incompressible, Navier-Stokes and continuity equations has been developed. Although it is based on the nodal integral approach and retains the high accuracy and high efficiency of methods based on that approach, it nevertheless overcomes the two major practical disadvantages of previously developed nodal integral methods. It is formulated directly in terms of velocities and pressures rather than velocities and normal stresses, and the final equations can be solved via simple velocity and pressure iterations rather than the Newton-Raphson iterations required by previously developed nodal integral methods. After the formulation of the method is presented, the results of its application to two time-dependent test problems, the inlet flow problem and the driven cavity problem, are reported.

1. INTRODUCTION

Previously developed nodal integral methods (NIMs) for the Navier-Stokes and continuity equations have proven to be highly accurate and highly efficient (Azmy, 1983), (Wilson, 1988) and (Decker, 1993). However, they were formulated in terms of the velocities and normal stresses as unknowns, and the resulting nonlinear discrete-variable equations were solved via Newton-Raphson iterations. They therefore were not practical for routine large-scale fluid dynamics computations. Thus, a method with the high accuracy of these NIMs that leads to discrete-variable equations that can be solved by a more conventional, less costly iteration scheme would be valuable. Further, it also would be useful if the method were formulated in terms of the primitive variables, i.e. with the velocity components and the pressure as the unknowns. Finally, it would be very convenient if the resulting discretized velocity components and pressures were associated with points in the computational domain that correspond to the locations of the discretized velocities and pressures of traditional finite-difference methods for fluid flow, which use shifted velocity grids (Domanus, 1983), so that the spatial stencils would be similar.

We have developed a new NIM for the time-dependent, incompressible, Navier-Stokes and continuity equations that uses velocities and pressures as unknowns, results in second-order errors for both the velocity and pressure variables, leads to a stencil similar to the staggered grid stencils employed in finite-difference methods and yields discrete-variable equations that can be solved via a simple iterative scheme that alternates between the velocity equations and the pressure equations. The formulation is a direct extension to the time-dependent case of the NIM we reported recently for the steady-state Navier-

Stokes and continuity equations (Michael, 2000a). It differs from another recently reported NIM (Wang, 2000) in that here the discrete-variable pressure unknowns are the node-averaged pressures and the equation for them is developed directly from the continuity equation by double averaging it over the node, whereas there the unknown pressures are the node surface-averaged pressures and the equations for them are developed using the Poisson equation for the pressure to arrive at equations which, of course, are quite different from those developed here.

2. FORMULATION OF THE NUMERICAL METHOD

Starting from the time-dependent two-dimensional continuity and Navier-Stokes equations (extension to 3-D is straightforward), the space-time computational domain is divided into I % J % N computational elements (nodes) each of volume $[-a_{i,j}, +a_{i,j}]$ % $[-b_{i,j}, +b_{i,j}]$ % $[-\tau, +\tau]$. (The subscript n on τ will be suppressed throughout this paper.) Transverse averaging the x momentum equation over y and t locally within the space-time node yields

$$\frac{d^2\overline{u}^{y,t}(x)}{dx^2} - \frac{\overline{u}^{y,t}(x)}{n_{i,j}}\frac{d\overline{u}^{y,t}(x)}{dx} = \overline{S}^{y,t}_{x\,i,j}(x) \tag{1}$$

where

$$\overline{S}^{y,t}_{x\,i,j}(x) = \frac{1}{2t}\int_{-t}^{+t} dt \frac{1}{2b_{i,j}}\int_{-b_{i,j}}^{+b_{i,j}} dy \left\{ \frac{1}{n}\left(\frac{\partial u(x,y,t)}{\partial t} + v(x,y,t)\frac{\partial u(x,y,t)}{\partial y} \right) - \frac{\partial^2 u(x,y,t)}{\partial y^2} - \frac{1}{n}\left(f_x(x,y,t) - \frac{\partial p(x,y,t)}{\partial x} \right) \right\}$$

and the x-component of the velocity and its first derivative, in the convection term, both have been expanded in Legendre polynomials in y and t and truncated at leading order, resulting in the average of their product being replaced by the product of their averages which, as shown previously in the context of the convection-diffusion equation (Michael, 2001), yields a second-order error at this stage of the development. Expanding both the velocity $\overline{u}^{y,t}(x)$ in the convection term on the left side of Eq. (1) and the pseudo-source term $\overline{S}^{y,t}_{x\,i,j}(x)$ on the right side in Legendre polynomials and truncating at leading order gives

$$\frac{d^2\overline{u}^{y,t}(x)}{dx^2} - u_{i,j}\frac{d\overline{u}^{y,t}(x)}{dx} = \overline{S}^{y,t}_{xo\,i,j} \tag{2}$$

where

$$u_{i,j} \equiv \overline{u}^{y,t,x}_{i,j} = \frac{1}{n_{i,j}}\frac{1}{2a_{i,j}}\int_{-a_{i,j}}^{+a_{i,j}} dx \frac{1}{2t}\int_{-t}^{+t} dt \frac{1}{2b_{i,j}}\int_{-b_{i,j}}^{+b_{i,j}} dy\, u(x,y,t)$$

and

$$\overline{S}^{y,t}_{xo\,i,j} = \frac{1}{2a_{i,j}} \int_{-a_{i,j}}^{+a_{i,j}} dx \, \frac{1}{2t} \int_{-t}^{+t} dt \, \frac{1}{2b_{i,j}} \int_{-b_{i,j}}^{+b_{i,j}} dy \left\{ \frac{1}{n} \left(\frac{\partial u(x,y,t)}{\partial t} + \nu(x,y,t) \frac{\partial u(x,y,t)}{\partial y} \right) - \frac{\partial^2 u(x,y,t)}{\partial y^2} - \frac{1}{n} \left(f_x(x,y,t) - \frac{\partial p(x,y,t)}{\partial x} \right) \right\}$$

which also results in a second order error (Michael, 2001). Integrating Eq. (2) twice from $-a_{i,j}$ to x, taking the limit of the upper bound of the outer integral as $x \to +a_{i,j}$ and solving for $d\overline{u}^{y,t}(-a_{i,j})/dx$ yields

$$\frac{d\overline{u}^{y,t}(-a_{i,j})}{dx} = \frac{u_{i,j}}{[e^{2u_{i,j}a_{i,j}} - 1]} \left[\overline{u}^{y,t}(+a_{i,j}) - \overline{u}^{y,t}(-a_{i,j}) \right] - \overline{S}^{y,t}_{xo\,i,j} \left\{ \frac{1}{u_{i,j}} - \frac{2a_{i,j}}{[e^{2u_{i,j}a_{i,j}} - 1]} \right\} \tag{3}$$

Analogously, integrating Eq. (2) twice from x to $+a_{i,j}$, taking the limit of the lower bound of the outer integral as $x \to -a_{i,j}$ and solving for $d\overline{u}^{y,t}(+a_{i,j})/dx$ gives

$$\frac{d\overline{u}^{y,t}(+a_{i,j})}{dx} = \frac{u_{i,j}}{[1 - e^{-2u_{i,j}a_{i,j}}]} \left[\overline{u}^{y,t}(+a_{i,j}) - \overline{u}^{y,t}(-a_{i,j}) \right] - \overline{S}^{y,t}_{xo\,i,j} \left\{ \frac{1}{u_{i,j}} - \frac{2a_{i,j}}{[1 - e^{-2u_{i,j}a_{i,j}}]} \right\} \tag{4}$$

Imposing the continuity of the y- and t-averaged normal stresses, the y- and t-averaged x velocity components and the y- and t-averaged pressures at the *(i-1,j)-(i,j)* and *(i,j)-(i+1,j)* node interfaces leads to

$$\frac{n_{i,j}u_{i,j}}{[1 - e^{-2u_{i,j}a_{i,j}}]} \overline{u}^{y,t}(a_{i-1,j}) - \left\{ \frac{n_{i,j}u_{i,j}}{[1 - e^{-2u_{i,j}a_{i,j}}]} + \frac{n_{i+1,j}u_{i+1,j}}{[e^{2u_{i,j}a_{i,j}} - 1]} \right\} \overline{u}^{y,t}(a_{i,j}) + \frac{n_{i+1,j}u_{i+1,j}}{[e^{2u_{i,j}a_{i,j}} - 1]} \overline{u}^{y,t}(a_{i+1,j}) = \overline{S}^{y,t}_{xo\,i+1,j} \left\{ \frac{1}{u_{i+1,j}} - \frac{2a_{i+1,j}}{[e^{2u_{i+1,j}a_{i+1,j}} - 1]} \right\} + \overline{S}^{y,t}_{xo\,i,j} \left\{ \frac{2a_{i,j}}{[1 - e^{-2u_{1,j}a_{1,j}}]} - \frac{1}{u_{i,j}} \right\} \tag{5}$$

To solve for the pseudo-source terms $\overline{S}^{y,t}_{xo\,i,j}$ and $\overline{S}^{y,t}_{xo\,i+1,j}$, needed on the right side, the uniqueness of the space-time node-averaged x velocity components, regardless of the order of averaging ($\overline{u}^{y,t,x}_{i,j} = \overline{u}^{x,t,y}_{i,j} = \overline{u}^{y,x,t}_{i,j}$), is imposed. To obtain an expression for $\overline{u}^{y,t,x}_{i,j}$, Eq. (2) is integrated twice from x to $+a_{i,j}$ and the expression for $d\overline{u}^{y,t}(+a_{i,j})/dx$ from Eq. (4) is substituted into the integrated equation. The resulting equation is transverse averaged over x and solved for $\overline{u}^{y,t,x}_{i,j}$ to obtain

$$\begin{aligned}\overline{u}^{y,t,x}_{i,j} &= \left\{1+\frac{1}{2u_{i,j}a_{i,j}}-\frac{1}{[1-e^{-2u_{i,j}a_{i,j}}]}\right\}\overline{u}^{y,t}(+a_{i,j})+\left\{\frac{1}{[1-e^{-2u_{i,j}a_{i,j}}]}-\frac{1}{2u_{i,j}a_{i,j}}\right\}\overline{u}^{y,t}(-a_{i,j})\\ &+\overline{S}^{y,t}_{xo\,i,j}\left\{\frac{1}{u^2_{i,j}}+\frac{a_{i,j}}{u_{i,j}}-\frac{2a_{i,j}}{u_{i,j}[1-e^{-2u_{i,j}a_{i,j}}]}\right\}\\ &= A^1_{i,j}\overline{u}^{y,t}(+a_{i,j})+A^2_{i,j}\overline{u}^{y,t}(-a_{i,j})+A^3_{i,j}\overline{S}^{y,t}_{xo\,i,j} \qquad (6)\end{aligned}$$

where the coefficients $A^m_{i,j}, m=1,2,3$, although obvious here, are given in the appendix. To obtain an expression for $\overline{u}^{y,x,t}_{i,j}$, the x-momentum equation is transverse averaged over y and x within the node to obtain an ODE in $\overline{u}^{y,x}_{i,j}(t)$. Then, the pseudo-source term in that ODE is expanded in Legendre polynomials and truncated at leading order. Finally, the resulting equation is solved for $\overline{u}^{y,x,t}_{i,j}$ to arrive at

$$\overline{u}^{y,x,t} = \frac{\overline{u}^{y,x}_{i,j}(+t)+\overline{u}^{y,x}_{i,j}(-t)}{2} \qquad (7)$$

Imposing the uniqueness of the space-time node-averaged x velocity component, i.e. equating Eqs. (6) and (7), and solving for $\overline{S}^{y,t}_{xo\,i,j}$ yields

$$\overline{S}^{y,t}_{xo\,i,j} = [A^3_{i,j}]^{-1}\left\{\frac{\overline{u}^{y,x}_{i,j}(+t)+\overline{u}^{y,x}_{i,j}(-t)}{2}-B^1_{i,j}\overline{u}^{y,t}(+a_{i,j})-B^2_{i,j}\overline{u}^{y,t}(-a_{i,j})\right\} \qquad (8)$$

where $B^1_{i,j}$ and $B^2_{i,j}$ are given in the appendix. To eliminate $\overline{u}^{y,x}_{i,j}(+t)$, the x momentum equation is averaged over y, x and t to obtain

$$\overline{S}^{y,t}_{xo\,i,j}+\overline{S}^{x,t}_{xo\,i,j} = \frac{\overline{u}^{y,x}_{i,j}(+t)-\overline{u}^{y,x}_{i,j}(-t)}{2\,tn_{i,j}}-\frac{1}{n_{i,j}}\left\{\overline{f}^{y,x,t}_{x\,i,j}-\frac{[\overline{p}^{y,t}(+a_{i,j})-\overline{p}^{y,t}(-a_{i,j})]}{2a_{i,j}}\right\} \qquad (9)$$

where $\overline{S}^{x,t}_{xo\,i,j}$ is the pseudo-source in the ODE that results from averaging the x momentum equation over x and t within the node. Then $\overline{S}^{y,t}_{xo\,i,j}$ from Eq. (8) and $\overline{S}^{x,t}_{xo\,i,j}$ from the analogous equation obtained using $\overline{u}^{x,t,y}_{i,j}$ and $\overline{u}^{y,x,t}_{i,j}$, are substituted into Eq. (9), and the resulting equation is solved for $\overline{u}^{y,x}_{i,j}(+t)$. Substituting the expression obtained for $\overline{u}^{y,x}_{i,j}(+t)$ into Eq. (8) yields

$$\overline{S}^{y,t}_{xo\,i,j} = \left\{R^1_{i,j}\overline{u}^{x,t}(b_{i,j}) + R^2_{i,j}\overline{u}^{x,t}(b_{i,j-1}) - L^1_{i,j}\overline{u}^{y,t}(a_{i,j}) - L^1_{i,j}\overline{u}^{y,t}(a_{i,j})\right\} - \frac{R^3_{i,j}}{n_{i,j}}\left[\frac{\overline{u}^{y,x}_{i,j}(-t)}{t} + \overline{f}^{ty,x,t}_{x\,i,j} - \frac{[\overline{p}^{y,t}(a_{i,j}) - \overline{p}^{y,t}(a_{i-1,j})]}{2a_{i,j}}\right] \tag{10}$$

where the explicit expressions for the coefficients are in the appendix. The expression for $\overline{S}^{x,t}_{xo\,i,j}$ is obtained analogously.

Substituting for the pseudo-source terms $\overline{S}^{y,t}_{xo\,i,j}$ and $\overline{S}^{y,t}_{xo\,i+1,j}$ from Eq. (10) with indices *(i,j)* and *(i+1,j)*, respectively, into Eq. (5) yields

$$\begin{aligned} &C^{y,t}_{i,j}\overline{u}^{y,t}(a_{i-1,j}) + D^{y,t}_{i,j}\overline{u}^{y,t}(a_{i,j}) + E^{y,t}_{i,j}\overline{u}^{y,t}(a_{i+1,j}) \\ &= A^5_{i+1,j}\left\{R^1_{i+1,j}\overline{u}^{x,t}(b_{i+1,j}) + R^2_{i+1,j}\overline{u}^{x,t}(b_{i+1,j-1}) - \frac{R^3_{i+1,j}}{n_{i+1,j}}\left(\frac{\overline{u}^{y,x}_{i+1,j}(-t)}{t} + \overline{f}^{y,x,t}_{x\,i+1,j}\right)\right\} \\ &+ A^6_{i,j}\left\{R^1_{i,j}\overline{u}^{x,t}(b_{i,j}) + R^2_{i,j}\overline{u}^{x,t}(b_{i,j-1}) - \frac{R^3_{i,j}}{n_{i+1,j}}\left(\frac{\overline{u}^{y,x}_{i,j}(-t)}{t} + \overline{f}^{y,x,t}_{x\,i,j}\right)\right\} \\ &+ \frac{A^5_{i+1,j}R^3_{i+1,j}}{n_{i+1,j}}\left(\frac{\overline{p}^{y,t}(a_{i+1,j}) - \overline{p}^{y,t}(a_{i,j})}{2a_{i+1,j}}\right) + \frac{A^6_{i,j}R^3_{i,j}}{n_{i,j}}\left(\frac{\overline{p}^{y,t}(a_{i,j}) - \overline{p}^{y,t}(a_{i-1,j})}{2a_{i,j}}\right) \end{aligned} \tag{11}$$

The coefficients in this equation and in those that follow are listed in the appendix. Equation (11) is a three-point equation for the $\overline{u}^{y,t}(a)$ in terms of the $\overline{u}^{x,t}(b)$, the $\overline{u}^{y,x}(t)$, and the space-time averaged node-surface pressures $\overline{p}^{y,t}(a)$. To express it in terms of the node-averaged pressure, two approximations are used. The first, already introduced, results from approximating the pressure gradients by constants, which was done when the pseudo sources were expanded in Legendre polynomials and truncated at leading order. This leads to

$$p_{i,j} \equiv \overline{p}^{x,y,t}_{i,j} = \frac{\overline{p}^{y,t}(a_{i,j}) + \overline{p}^{y,t}(a_{i-1,j})}{2} \tag{12}$$

Solving this equation, with indices *(i,j)* and *(i+1,j)*, for $\bar{p}^{y,t}(a_{i-1,j})$ and $\bar{p}^{y,t}(a_{i+1,j})$, substituting into Eq. (11), and using a second approximation $\bar{p}^{y,t}(a_{i,j}) = (p_{i,j} + p_{i+1,j})/2$, which also leads to a second-order error (for a uniform grid), gives

$$C_{i,j}^{y,t}\bar{u}^{y,t}(a_{i-1,j}) + D_{i,j}^{y,t}\bar{u}^{y,t}(a_{i,j}) + E_{i,j}^{y,t}\bar{u}^{y,t}(a_{i+1,j}) = F_{i,j}^{y,t} + \left(\frac{A_{i,j}^6 R_{i,j}^3}{n_{i,j}} + \frac{A_{i+1,j}^5 R_{i+1,j}^3}{n_{i+1,j}}\right)\left[\frac{p_{i+1,j} - p_{i,j}}{2a}\right] \tag{13}$$

where

$$F_{i,j}^{y,t} = A_{i+1,j}^5\left\{R_{i+1,j}^1\bar{u}^{x,t}(b_{i+1,j}) + R_{i+1,j}^2\bar{u}^{x,t}(b_{i+1,j-1}) - \frac{R_{i+1,j}^3}{n_{i+1,j}}\left[\frac{\bar{u}_{i+1,j}^{y,x}(-t)}{t} + \bar{f}_{x\,i+1,j}^{y,x,t}\right]\right\}$$
$$+ A_{i,j}^6\left\{R_{i,j}^1\bar{u}^{x,t}(b_{i,j}) + R_{i,j}^2\bar{u}^{x,t}(b_{i,j-1}) - \frac{R_{i,j}^3}{n_{i,j}}\left[\frac{\bar{u}_{i,j}^{x,y}(-t)}{t} + \bar{f}_{x\,i,j}^{y,x,t}\right]\right\}$$

Equation (13) is the final three-point equation for the $\bar{u}^{y,t}(a)$ in terms of the node-averaged pressures $p_{i,j}$ (and the $\bar{u}^{x,t}(b)$ and the $\bar{u}^{y,x}(t)$). A similar three-point equation for $\bar{u}^{x,t}(b)$ is obtained from the x- and t-averaged x momentum equation. In both these three-point equations, the coefficients depend upon the node-averaged x velocity component $u_{i,j} \equiv \bar{u}_{i,j}^{y,t,x}$ defined below Eq. (2), and the node-averaged y velocity component $v_{i,j} = \bar{v}_{i,j}^{x,t,y}$, that result from the convection terms in the x momentum equation. These are taken as known during the iterative solution of the three-point equations. But since they are updated after these equations are solved, expressions for them are required. The expression for $\bar{u}_{i,j}^{y,t,x}$ is obtained by substituting for $\bar{S}_{xo\,i,j}^{y,t}$ from Eq. (10) into Eq. (6) and using the pressure approximations above to obtain

$$\bar{u}_{i,j}^{y,t,x} = A_{i,j}^3\left(R_{i,j}^1\bar{u}^{x,t}(b_{i,j}) + R_{i,j}^2\bar{u}^{x,t}(b_{i,j-1})\right) + B_{i,j}^3\left(L_{i,j}^1\bar{u}^{y,t}(a_{i,j}) + L_{i,j}^2\bar{u}^{y,t}(a_{i-1,j})\right)$$
$$- \frac{A_{i,j}^3 R_{i,j}^3}{n_{i,j}}\left\{\frac{\bar{u}_{i,j}^{y,x}(-t)}{t} + \bar{f}_{xi,j}^{y,x,t} - \frac{[p_{i+1,j} - p_{i,j}]}{2a}\right\} \tag{14}$$

Equations for $\bar{v}^{x,t}(b_{i,j})$, $\bar{v}^{y,t}(a_{i,j})$ and $\bar{v}_{i,j}^{x,y,t}$ are obtained analogously from the y momentum equation.

Equations for the $\overline{u}^{y,x}_{i,j}(+t)$ and $\overline{v}^{x,y}_{i,j}(+t)$, needed as the additional velocity equations for the time advancement of the solutions for the velocity components, are obtained by x- and y-averaging the x momentum and y momentum equations and solving the resulting ODEs in time. [Since these are simple first order equations in time, they are equivalent to the equations obtained by triple averaging the x and y momentum equations (in x, y and t). For example, the equation for $\overline{u}^{y,x}_{i,j}(+t)$ is equivalent to Eq. (9), which was used in conjunction with the two equations that resulted from imposing the uniqueness $\overline{u}^{y,t,x}_{i,j} = \overline{u}^{x,t,y}_{i,j} = \overline{u}^{y,x,t}_{i,j}$ to eliminate the two pseudo-sources $\overline{S}^{y,t}_{xo\,i,j}$ and $\overline{S}^{x,t}_{xo\,i,j}$ and $\overline{u}^{y,x}_{i,j}(+t)$. Of course, this same equation, Eq. (9), can be used to generate the expression for $\overline{u}^{y,x}_{i,j}(+t)$ which it had been previously used to eliminate.] The resulting equation obtained for $\overline{u}^{y,x}_{i,j}(+t)$, after eliminating $\overline{S}^{y,t}_{xo\,i,j}$ via Eq. (10) and $\overline{S}^{x,t}_{xo\,i,j}$ via its analogue, and rewriting the node surface-averaged pressures $\overline{p}^{y,t}(+a_{i,j})$ and $\overline{p}^{y,t}(-a_{i,j})$ in terms of the node averaged pressures via Eq. (12), is

$$\overline{u}^{y,x}_{i,j}(+t) = 2\left\{A^3_{i,j}\left(R^1_{i,j}\overline{u}^{x,t}(b_{i,j}) + R^2_{i,j}\overline{u}^{x,t}(b_{i,j-1})\right) + B^3_{i,j}\left(L^1_{i,j}\overline{u}^{y,t}(a_{i,j}) + L^2_{i,j}\overline{u}^{y,t}(a_{i-1,j})\right)\right.$$
$$\left. - \frac{A^3_{i,j}R^3_{i,j}}{n_{i,j}}\left[\overline{f}^{y,x,t}_{x\,i,j} - \frac{p_{i+1,j} - p_{i,j}}{2a_{i,j}}\right] - \frac{1}{2}\left[L^3_{i,j} + R^3_{i,j} + \frac{A^3_{i,j}R^3_{i,j}}{t\,n_{i,j}}\right]\overline{u}^{y,x}_{i,j}(-t)\right\} \qquad (15)$$

This equation, and the analogous equation for $\overline{v}^{x,y}_{i,j}(+t)$ are the two additional velocity equations used for the time advancement of the velocity solutions.

Finally, to obtain an equation for the node-averaged pressures, the continuity equation is locally averaged over x, y and t within a space-time node to obtain

$$\frac{\overline{u}^{y,t}(a_{i,j}) - \overline{u}^{y,t}(a_{i-1,j})}{2a} + \frac{\overline{v}^{x,t}(b_{i,j}) - \overline{v}^{x,t}(b_{i,j-1})}{2b} = 0 \qquad (16)$$

Solving Eq. (13) for $\overline{u}^{y,t}(a_{i,j})$ and its *(i-1,j)* analogue for $\overline{u}^{y,t}(a_{i-1,j})$, and the analogous equations for $\overline{v}^{x,t}(b_{i,j})$ and $\overline{v}^{x,t}(b_{i,j-1})$, and substituting into Eq. (16) yields the five-point pressure equation for the node-averaged pressures

$$
\begin{aligned}
&K^L_{i,j}p_{i-1,j} + K^B_{i,j}p_{i,j-1} + K^C_{i,j}p_{i,j} + K^R_{i,j}p_{i+1,j} + K^A_{i,j}p_{i,j+1} \\
&= \frac{1}{2aD^{t,y}_{i,j}}\left[F^{\bar{u}^{t,y}}_{LPi,j} - C^{t,y}_{i,j}\bar{u}^{t,y}(a_{i-1,j}) - D^{t,y}_{i,j}\bar{u}^{t,y}(a_{i+1,j})\right] \\
&+ \frac{1}{2aD^{t,y}_{i-1,j}}\left[F^{\bar{u}^{t,y}}_{LPi-1,j} - C^{t,y}_{i-1,j}\bar{u}^{t,y}(a_{i-2,j}) - D^{t,y}_{i-1,j}\bar{u}^{t,y}(a_{i,j})\right] \\
&+ \frac{1}{2bD^{t,x}_{i,j}}\left[F^{\bar{v}^{t,x}}_{LPi,j} - C^{t,x}_{i,j}\bar{v}^{t,x}(b_{i,j-1}) - D^{t,x}_{i,j}\bar{v}^{t,x}(b_{i,j+1})\right] \\
&+ \frac{1}{2bD^{t,x}_{i,j-1}}\left[F^{\bar{v}^{t,x}}_{LPi,j-1} - C^{t,x}_{i,j-1}\bar{v}^{t,x}(b_{i,j-2}) - D^{t,x}_{i,j-1}\bar{v}^{t,x}(b_{i,j})\right] \qquad (17)
\end{aligned}
$$

where the coefficients are given in the appendix.

Equation (13) for the $\bar{u}^{y,t}(a_{i,j})$ and the related equations for the $\bar{u}^{x,t}(b_{i,j})$, $\bar{v}^{x,t}(b_{i,j})$ and $\bar{v}^{y,t}(a_{i,j})$ are the spatially discretized equations for the node (space-time) surface-averaged velocity components, Eq. (16) for $\bar{u}^{y,x}_{i,j}(t)$ and its analogue for $\bar{v}^{x,y}_{i,j}(t)$ are the temporally discretized equations for the node (space-space) surface-averaged velocity components, and Eq. (17) for the $p_{i,j} \equiv \bar{p}^{x,y,t}_{i,j}$ is the equation for the node (space-space-time) volume-averaged pressures. The $\bar{u}^{y,t}(a_{i,j})$, $\bar{u}^{x,t}(b_{i,j})$, $\bar{v}^{x,t}(b_{i,j})$ and $\bar{v}^{y,t}(a_{i,j})$ are defined on node spatial surfaces $a_{i,j}$ and $b_{i,j}$ which correspond to the locations occupied by velocity components on the standard shifted velocity grids used in finite difference schemes (although two velocity components appear at each location here), and the $p_{i,j} \equiv \bar{p}^{x,y,t}_{i,j}$ are defined over the node space-time volumes which correspond to the locations occupied by pressures on the standard non-shifted pressure grids used in finite-difference schemes. Thus, the objective of developing a nodal integral method for fluid dynamics equations in terms of primitive variables, the velocities and pressures, with a stencil similar to that for a finite-difference scheme for the Navier-Stokes equations, has been achieved.

The velocity and pressure equations developed here apply to nodes that are in the interior of the computational domain. Naturally, they differ slightly for nodes that are adjacent to the boundaries of the domain. The details of these differences, along with a more detailed development of the domain interior equations are available elsewhere (Michael, 2000b).

3. NUMERICAL RESULTS

To implement the new NIM, the velocity and pressure equations developed in Sec. 2, are solved iteratively as follows. At the beginning of a time step $\bar{u}^{y,x}_{i,j}(-t)$ and $\bar{v}^{x,y}_{i,j}(-t)$ are set equal to their values at the end of the previous time step, or if it is the first time

step, equal to their initial values. In the first time step $\bar{u}^{y,t}(a_{i,j})$, $\bar{v}^{x,t}(b_{i,j})$, $\bar{u}^{x,t}(b_{i,j})$, $\bar{v}^{y,t}(a_{i,j})$ and $p_{i,j}$ are initially approximated by $\bar{u}^{y}(a_{i,j},t=0)$, $\bar{v}^{x}(b_{i,j},t=0)$, $\bar{u}^{x}(b_{i,j},t=0)$, $\bar{v}^{y}(a_{i,j},t=0)$ and $\bar{p}^{x,y}_{i,j}(t=0)$; in subsequent time steps they are initially approximated by the values computed in the previous time step. Then $\bar{u}^{y,t,x}_{i,j}$ and $\bar{v}^{x,t,y}_{i,j}$ are calculated and used to generate the coefficients that appear in the velocity and pressure equations. This marks the beginning of the outer iterations (iterations due to the non-linearity of the equations) within the time step. Next, the system of equations, along with the appropriate boundary equations, is solved iteratively (inner iterations) to obtain $\bar{u}^{y,t}(a_{i,j})$, $\bar{v}^{x,t}(b_{i,j})$, $\bar{u}^{x,t}(b_{i,j})$, $\bar{v}^{y,t}(a_{i,j})$ and $p_{i,j}$. These computed values are used to update the space-time node-averaged velocities. New coefficients based on the updated $\bar{u}^{y,t,x}_{i,j}$ and $\bar{v}^{x,t,y}_{i,j}$ are computed and the residual of the system of equations is calculated and its convergence is checked. If convergence has not been achieved, a new outer iteration begins and the process is repeated until convergence is achieved. Otherwise, the calculations for the time step stop and the converged values are used to calculate $\bar{u}^{y,x}_{i,j}(+t)$ and $\bar{v}^{x,y}_{i,j}(+t)$, and calculations for the next time step begin.

To test the new method two time-dependent problems were solved. A time-dependent version of the inlet flow problem was solved first to provide a basic test. Then, a time-dependent driven cavity problem, which is widely used in its steady-state form as a challenging test for numerical methods, was solved. The iterative convergence criteria used in both these calculations were 10^{-8} on the outer iterations and 10^{-12} on the inner iterations, and because of the previously established high accuracy of the method on coarse spatial meshes (Michael, 2000a), (Michael, 2000b), they were done using 8×8 meshes.

3.1 Inlet Flow Problem

In the inlet flow problem, which was solved for Re = 10, the flow is taken initially as a slug of fluid moving between horizontal parallel plates with a uniform velocity that is equal to the inlet flow velocity; then at t = 0, no-slip boundary conditions are applied at the top and bottom plates. This causes the fluid to decelerate near the plates, and because of incompressibility, more fluid is pushed to the center region thus causing it to accelerate near the channel center. This problem has no known exact analytical solution in either its time-dependent or steady-state form, but flow maps can be generated and examined to determine whether the general transient behavior of the fluid is properly calculated and whether the velocity and pressure fields calculated for long times agree with the stable steady-state distributions. The steady-state form of this problem has been solved by several numerical methods (Hirt, 1975), (Horak, 1981), (Azmy, 1983), (Azmy, 1984) including our previously developed new steady-state NIM (Michael, 2000a). Hence, the computed long time-solution of the time-dependent problem can be compared with the numerical results from the steady-state NIM. The geometry, parameters, and boundary and initial conditions for this time-dependent problem are given in Fig. 1. The flow maps that resulted from calculations done via the new NIM on an 8 % 8 spatial mesh using a time

step $\Delta t = 0.1$ are shown in Figs. 2 and 3 for times 0.1 and 15 and using $\Delta t = 20.0$ in Fig. 4 for t = 20000.

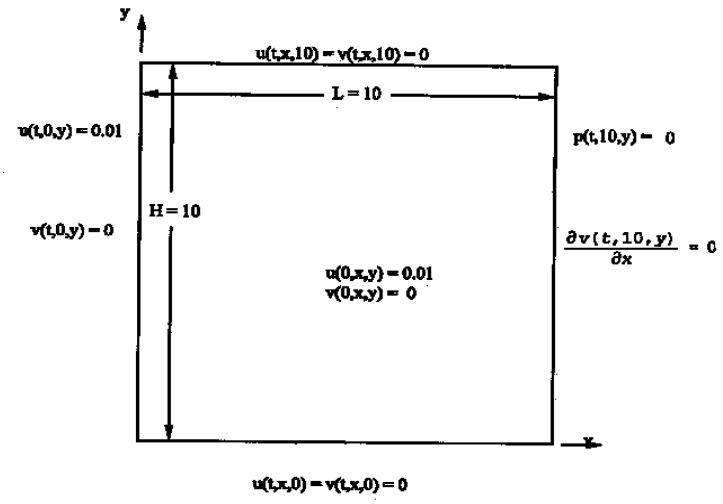

Fig. 1 The dimensions and the boundary and initial conditions for the time-dependent inlet flow problem.

The flow maps show that the calculated behavior of the fluid is qualitatively correct. As shown in Figs. 2 and 3, very early in the transient (at t = 0.1) the flow is very much like slug flow in accordance with the initial condition. As time progresses the fluid near the two plates slows down, while in the center region it accelerates as shown in Fig. 3 for t = 15. Finally, at t = 20000, the fluid near the plates has decelerated to a very small velocity, the flow at the inlet converges strongly toward the center of the channel, and the velocity field has almost reached its time-asymptotic state, as is evident from comparison of Fig. 4 with Fig. 5, which shows the solution to the steady-state problem, calculated using our recently reported new steady-state NIM on the same grid.

A quantitative estimate of the accuracy, at least of the long-time solution, can be made by calculating the difference between the solution at long-time and the stable steady-state solution computed on the same mesh. To this end, the average L_1 difference (not error but difference) between the steady-state solution (node-averaged velocity components and node-averaged pressure) computed using an 8 % 8 mesh and the time-dependent solution computed at t = 20000 using the same 8 % 8 mesh has been calculated — even though the latter of course is not truly time-asymptotic. This average percent L_1 relative difference was 0.2694%. Assuming there is not a fortuitous cancellation between the error due to the time advancement in the NIM and the difference in the solution at t = 20000 and the time-asymptotic solution, this shows that the long-time solution generated by the full space-time NIM is in good agreement with that generated by the NIM for the steady-state Navier-Stokes equations, whose accuracy has been previously established (Michael, 2000a), (Michael, 2000b).

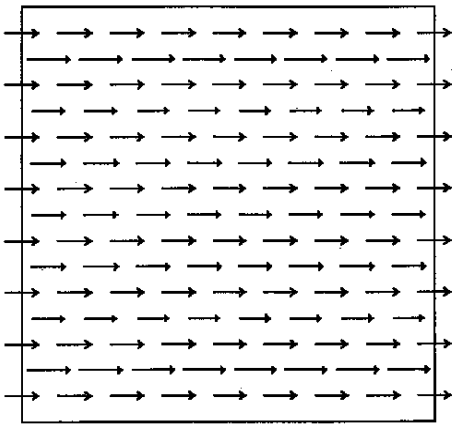

Fig. 2 The inlet flow problem velocity field calculated at t = 0.1 on an 8 % 8 mesh with time step $\Delta t = 0.1$ (Re = 10.0).

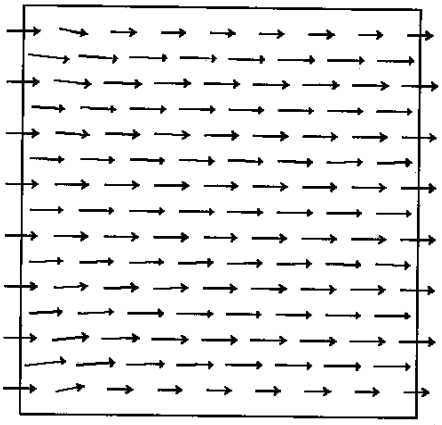

Fig. 3 The inlet flow problem velocity field calculated at t = 15.0 on an 8 % 8 mesh with time step $\Delta t = 0.1$ (Re = 10.0).

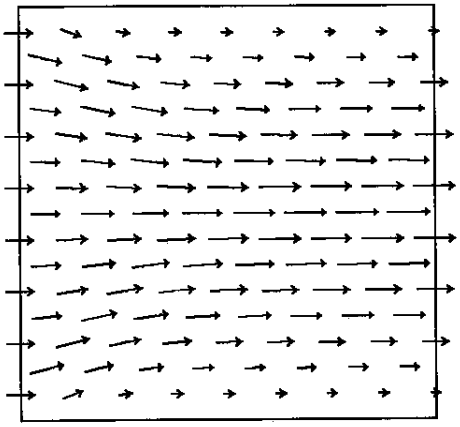

Fig. 4 The inlet flow problem velocity field calculated at t = 20000 on an 8 % 8 mesh with time step $\Delta t = 20.0$ (Re = 10.0).

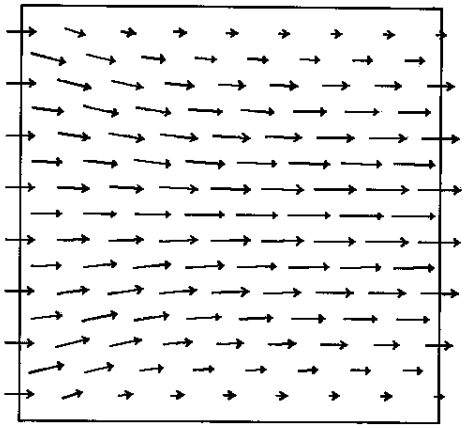

Fig. 5 The steady-state inlet flow problem velocity field calculated on an 8 % 8 mesh (Re = 10.0).

3.2 Driven Cavity Problem

In the second test problem studied, the time-dependent driven cavity problem, the viscous fluid is initially at rest, and the top plate suddenly moves (at t = 0) at constant speed from left to right causing fluid motion inside the cavity. Neither the steady-state nor the time-dependent form of this problem has a known exact analytical solution. However, the steady-state problem has been extensively studied theoretically, experimentally and numerically (Burgraf, 1966), (Pan, 1967), (Bozeman, 1973), (Hirt, 1975), (Taneda, 1979), (Ghia, 1982), (Schriber, 1983), (Azmy, 1984), (Kossef, 1985), (Michael, 2000a) and (Michael, 2000b); thus, the numerical solutions of the time-dependent driven cavity problem reported below can be compared at long-times with the stable steady-state solutions.

Velocity fields for the time-dependent driven cavity problem with Re = 300, computed at several times via the new NIM on an 8 % 8 mesh, are shown in Figs. 6-9. The flow map in Fig. 6 shows that at t = 1.0, the fluid is re-circulating as a single primary vortex. At t = 2.5, the secondary vortex has already started to develop in the lower downstream corner (Fig. 7), but the flow has not yet reached its time-asymptotic state. Finally, when t = 1000.0 (Fig. 8), the secondary vortex appears to have developed fully, and the fluid appears to have reached its time-asymptotic velocity distribution. As in the case of the time-dependent inlet flow problem discussed in subsection 3.1, the fact that the computed transient behavior of the velocity field for the driven cavity problem exhibits the correct physical behavior indicates that the numerical solution generated by the new NIM for this problem is qualitatively correct. The average percent L_1 relative difference based on the time-dependent NIM solution at t = 1000 (velocity field shown in Fig. 8), and the steady-state NIM solution (Fig. 9), both obtained using an 8 % 8 spatial mesh, was 0.05%. Again as in subsection 3.1, assuming there is not a fortuitous cancellation of the error that results from the time advancement in the NIM with the difference between the solution at t = 1000.0 and the time-asymptotic solution, the results from the space-time NIM agree well with those produced by the steady-state NIM, the accuracy of which was demonstrated earlier (Michael, 2000a), (Michael, 2000b) where in the context of the steady-state driven cavity problem it was shown that the new steady-state NIM accurately predicted the height of the secondary vortex (a frequently used measure of the accuracy of a new numerical method for fluid flow) even on coarse meshes.

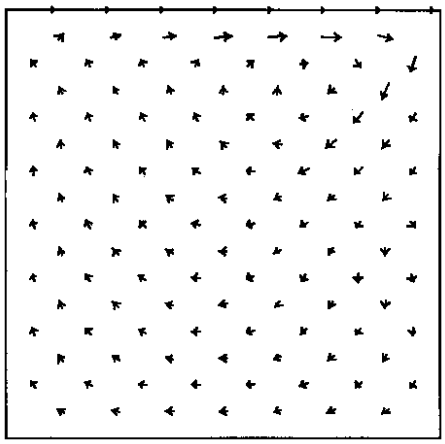

Fig. 6 The driven cavity problem velocity field calculated at t = 1.0 on an 8×8 mesh with time step $\Delta t = 0.1$ (Re = 300.0).

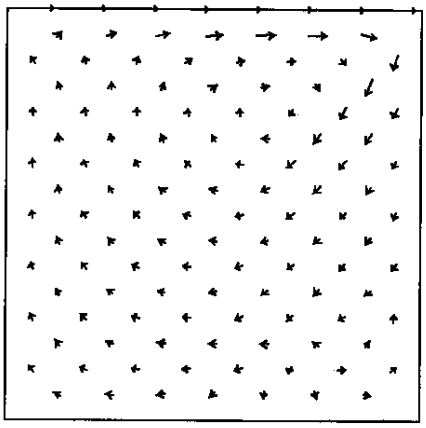

Fig. 7 The driven cavity problem velocity field calculated at t = 2.5 on an 8×8 mesh with time step $\Delta t = 0.1$ (Re = 300.0).

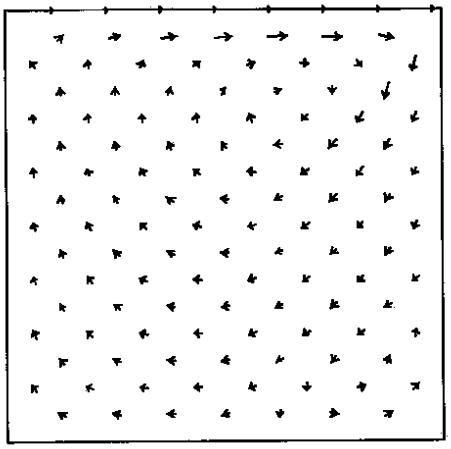

Fig. 8 The driven cavity problem velocity field calculated at t = 1000.0 on an 8 % 8 mesh with time step Δt = 4.0 (Re = 300.0).

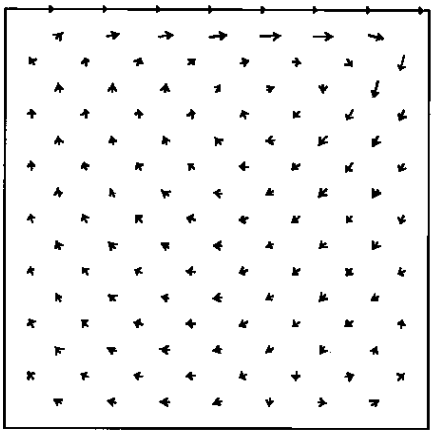

Fig. 9 The steady-state driven cavity problem velocity field calculated on an 8 % 8 mesh (Re = 300.0).

4. CONCLUSIONS

A new primitive-variable nodal integral method has been developed for the time-dependent, incompressible, Navier-Stokes and continuity equations, and it has been applied to two test problems, the inlet flow problem and the driven cavity problem, to demonstrate its accuracy. The formulation results in second-order errors in both the velocity and pressure variables, and a spatial stencil for the discretized velocities and pressures that is very similar to those that arise in widely used finite-difference methods based on shifted velocity grids (Domanus, 1983); it also eliminates the use of normal stresses (rather than pressures) as unknowns and the need to solve the final equations by Newton-Raphson iterations. Thus, the new method overcomes the two major drawbacks of the original nodal integral methods for fluid flow (Azmy, 1983), (Wilson, 1988) (Decker, 1993) while retaining their high accuracy and computational efficiency.

APPENDIX

The explicit expressions for the coefficients $A_{i,j}^m, m = 1,...,8$ and $B_{i,j}^m, m = 1,...,8$ that appear in Eqs. (6), (8), (11), (13), (14) and (16) are

$$A_{i,j}^1 = \left\{ 1 + \frac{1}{2u_{i,j}a_{i,j}} - \frac{1}{[1-e^{-2u_{i,j}a_{i,j}}]} \right\}; \qquad B_{i,j}^1 = \left\{ 1 + \frac{1}{2v_{i,j}b_{i,j}} - \frac{1}{[1-e^{-2v_{i,j}b_{i,j}}]} \right\};$$

$$A_{i,j}^2 = \left\{ \frac{1}{[1-e^{-2u_{i,j}a_{i,j}}]} - \frac{1}{2u_{i,j}a_{i,j}} \right\}; \qquad B_{i,j}^2 = \left\{ \frac{1}{[1-e^{-2v_{i,j}b_{i,j}}]} - \frac{1}{2v_{i,j}b_{i,j}} \right\};$$

$$A_{i,j}^3 = \left\{ \frac{1}{u_{i,j}^2} + \frac{a_{i,j}}{u_{i,j}} - \frac{2a_{i,j}}{u_{i,j}[1-e^{-2u_{i,j}a_{i,j}}]} \right\}; \qquad B_{i,j}^3 = \left\{ \frac{1}{v_{i,j}^2} + \frac{b_{i,j}}{v_{i,j}} - \frac{2b_{i,j}}{v_{i,j}[1-e^{-2v_{i,j}b_{i,j}}]} \right\};$$

$$A_{i,j}^4 = \frac{n_{i,j}u_{i,j}}{[e^{2u_{i,j}a_{i,j}}-1]}; \qquad B_{i,j}^4 = \frac{n_{i,j}v_{i,j}}{[e^{2v_{i,j}b_{i,j}}-1]};$$

$$A_{i,j}^5 = n_{i,j}\left\{ \frac{1}{u_{i,j}} - \frac{2a_{i,j}}{[e^{2u_{i,j}a_{i,j}}-1]} \right\}; \qquad B_{i,j}^5 = n_{i,j}\left\{ \frac{1}{v_{i,j}} - \frac{2b_{i,j}}{[e^{2v_{i,j}b_{i,j}}-1]} \right\};$$

$$A_{i,j}^6 = n_{i,j}\left\{ \frac{2a_{i,j}}{[1-e^{-2u_{i,j}a_{i,j}}]} - \frac{1}{u_{i,j}} \right\}; \qquad B_{i,j}^6 = n_{i,j}\left\{ \frac{2b_{i,j}}{[1-e^{-2v_{i,j}b_{i,j}}]} - \frac{1}{v_{i,j}} \right\};$$

$$A_{i,j}^7 = \frac{n_{i,j}u_{i,j}}{[1-e^{-2u_{i,j}a_{i,j}}]}; \qquad B_{i,j}^4 = \frac{n_{i,j}v_{i,j}}{[1-e^{-2v_{i,j}b_{i,j}}]};$$

$$A_{i,j}^8 = \left\{ 1 - \frac{A_{i,j}^3}{n_{i,j}t} \right\}; \qquad B_{i,j}^8 = \left\{ 1 - \frac{B_{i,j}^3}{n_{i,j}t} \right\};$$

The coefficients $C_{i,j}^{y,t}$, $D_{i,j}^{y,t}$, $E_{i,j}^{y,t}$, $L_{i,j}^r$ and $R_{i,j}^r$, r = 1, 2, 3, which appear in Eqs. (11), (13), (14), (16) and (17) are

$$C_{i,j}^{y,t} = A_{i,j}^7 + A_{i,j}^6 L_{i,j}^2 B_{i,j}^8$$
$$D_{i,j}^{y,t} = -A_{i,j}^7 - A_{i+1,j}^4 + A_{i,j}^6 L_{i,j}^1 B_{i,j}^8 + A_{i+1,j}^5 L_{i+1,j}^2 B_{i+1,j}^8$$
$$E_{i,j}^{y,t} = A_{i+1,j}^4 + A_{i+1,j}^5 L_{i+1,j}^1 B_{i+1,j}^8$$

where

$$L_{i,j}^k = A_{i,j}^k \left[A_{i,j}^3 + B_{i,j}^3 - \frac{A_{i,j}^3 B_{i,j}^3}{n_{i,j}t} \right]^{-1}, k = 1,2,3.$$

and

$$R_{i,j}^k = B_{i,j}^k \left[A_{i,j}^3 + B_{i,j}^3 - \frac{A_{i,j}^3 B_{i,j}^3}{n_{i,j}t} \right]^{-1}, k = 1,2,3.$$

Finally, the “left”, “below”, “center”, “right” and “above” coefficients in Eq. (17) are given by

$$K_{i,j}^L = \frac{1}{2aD_{i-1,j}^{t,y}} \left[\frac{A_{i,j}^5 R_{i,j}^3}{n_{i,j}} + \frac{A_{i-1,j}^6 R_{i-1,j}^3}{n_{i-1,j}} \right];$$

$$K_{i,j}^{B} = \frac{1}{2bD_{i,j-1}^{t,x}}\left[\frac{B_{i,j}^{5}L_{i,j}^{3}}{n_{i,j}} + \frac{B_{i,j-1}^{6}L_{i,j-1}^{3}}{n_{i,j-1}}\right];$$

$$K_{i,j}^{R} = \frac{1}{2aD_{i,j}^{t,y}}\left[\frac{A_{i+1,j}^{5}R_{i+1,j}^{3}}{n_{i+1,j}} + \frac{A_{i,j}^{6}R_{i,j}^{3}}{n_{i,j}}\right];$$

$$K_{i,j}^{A} = \frac{1}{2bD_{i,j}^{t,x}}\left[\frac{B_{i,j+1}^{5}L_{i,j+1}^{3}}{n_{i,j+1}} + \frac{B_{i,j}^{6}L_{i,j}^{3}}{n_{i,j}}\right];$$

$$K_{i,j}^{C} = -\left[K_{i,j}^{L} + K_{i,j}^{B} + K_{i,j}^{R} + K_{i,j}^{A}\right].$$

REFERENCES

Azmy, Y. Y., Dorning, J. J., 1983. A nodal integral approach to the numerical solution of partial differential equations. In: *Advances in Reactor Computations*, Vol. II, American Nuclear Society, LaGrange Park, Illinois, pp. 893-909.

Azmy, Y. Y., Dorning, J. J., 1984. Arc-length continuation of nodal integral method solutions to the nonlinear Navier-Stokes equations. In: Taylor, C., Hinton, E., Owen, D.R.J., Onate, E. (Eds.), *Numerical Methods for Nonlinear Problems*, Vol. II, Pineridge Press, Swansea, UK., pp. 672-687.

Bozeman, J. D., Dalton, C., 1973. Numerical study of viscous flow in a cavity. *J. Comp. Phys.*, **12**, 348-363.

Burgraf, O. R., 1966. Analytical and numerical studies of the structure of steady separated flows. *J. Fluid Mech.*, **24**, 113-151.

Decker, W. J., Dorning, J. J., 1993. A block iterative nodal integral method for fluid dynamics problems. In: Küsters, H., Stein, E., Werner, W. (Eds.), *Joint Int. Conf. On Math. Methods and Supercomputing in Nuclear Appl.*, Kernforschungszentrum Karlsruhe GmbH, Karlsruhe, Germany, pp. 208-223.

For example see: Domanus, H. M., Schmitt, R. C., Shah, W. T., Shah, V. L. COMMIX-1A: A three dimensional transient single-phase computer program for thermal hydraulic analysis of single and multi component systems: Vol. I: User's Manual, and Vol. II: Assessment and Verification, NUREG/CR-2896, ANL-82-25, Dec. 1983.

Ghia, U., Ghia, K. N., Shin, C. T., 1982. High-Re solutions for incompressible flow using the Navier-Stokes equations and a multigrid method. *J. Comp. Phys.*, **48**, 387-

Hirt, W. C., Nicholas, B. D., Romero, N. C., SOLA - A numerical algorithm for transient fluid flows, LA-852, 1975.

Horak, W. C., Dorning, J. J., 1981. A nodal Green's tensor method for the efficient numerical solution of laminar flow problems. In: Taylor, C, Schrefler, B. A. (Eds.), *Numerical Methods in Laminar and Turbulent Flow*, Vol. II, Pineridge Press, Swansea, UK., pp. 103-112. See also: Horak, W. C., Dorning, J. J., 1985. A nodal coarse-mesh method for the efficient numerical solution of laminar flow problems. *J. Comp. Phys.*, **59**, 405-450.

Kossef, J. R., Street, R. L., 1985. On end wall effects in a lid-driven cavity flow. *J. Fluid Eng.*, **106**, 385-389.

Michael, E. P. E., Dorning, J., 2000a. A primitive-variable nodal method for the steady-state Navier-Stokes equations. *Trans. Am. Nucl. Soc.*, **83,** 420-422.

Michael, E. P. E., New nodal methods for fluid flow equations, Ph.D. dissertation, University of Virginia, 2000b.

Michael, E. P. E., Dorning, J., Rizwan-uddin, 2001. Studies on nodal integral methods for the convection-diffusion equation. *Nucl. Sci. Eng*., **137**, 380-399.

Pan, F., Acrivos, A., 1967. Steady flows in rectangular cavities. *J. Fluid. Mech.,* **28**, 643-655.

Schreiber, R., Keller, H. B., 1983. Driven cavity flows by efficient numerical techniques. *J. Comp. Phys.*, **49**, 310. See also: Schreiber, R., Keller, H. B., 1983. Spurious solutions in driven cavity calculations. *J. Comp. Phys.*, **49**, 165.

Taneda, S., 1979. Visualization of separating Stokes flows. *J. Phys. Soc. Jpn.*, **46**, 1935-1942. See also: Van Dyke, M., 1982. *An Album of Fluid Motion,* The Parabolic Press, Stanford, CA.

Wang, F., Rizwan-uddin, 2000. A nodal scheme for the time-dependent, incompressible Navier-Stokes equations. *Trans. Am. Nucl. Soc*., **83**, 422-424.

Wilson, G. L, Rydin, R. A., Azmy, Y. Y., 1988. Time-dependent nodal integral method for the investigation of bifurcation and nonlinear phenomena in fluid flow. *Nucl. Sci. Eng.*, **100**, 414.